Methane Hydrate: Killer cause of Earth's greatest mass extinction

Uwe Brand [a, *], Nigel Blamey [a], Claudio Garbelli [b, **], Erika Griesshaber [c], Renato Posenato [d], Lucia Angiolini [b], Karem Azmy [e], Enzo Farabegoli [f], Rosemarie Came [g]

[a] Department of Earth Sciences, Brock University, 1812 Sir Isaac Brock Way, St. Catharines, Ontario L2S 3A1, Canada

[b] Dipartimento di Scienze della Terra, Via Mangiagalli 34, Università di Milano, 20133 Milan, Italy

[c] Department of Earth and Environment Sciences, Ludwig Maximilian Universität, Theresienstr. 41, 80333 München, Germany

[d] Dipartimento di Fisica e Scienze della Terra, Università di Ferrara, Polo Scientifico-tecnologico, Via Saragat 1, 44100 Ferrara, Italy

[e] Department of Earth Sciences, Memorial University, St. John's, NL A1B 3X5, Canada

[f] Dipartimento di Scienze della Terra e Geologico – Ambientali, Università di Bologna, Via Zamboni 67, 40126 Bologna, Italy

[g] Department of Earth Sciences, The University of New Hampshire, Durham, New Hampshire 03824, USA

* Corresponding author. *E-mail address*: uwe.brand@brocku.ca, ubrand@brocku.ca

** Present address: State Key Laboratory of Paleobiology and Stratigraphy, Nanjing Institute of Geology and Paleontology, Chinese Academy of Sciences, Nanjing, Jiangsu 210008, P.R. China

Abstract

The cause for the end Permian mass extinction, the greatest challenge life on Earth faced in its geologic history, is still hotly debated by scientists. The most significant marker of this event is the negative $\delta^{13}C$ shift and rebound recorded in marine carbonates with a duration ranging from 2000 to 19 000 years depending on localities and sedimentation rates. Leading causes for the event are Siberian trap volcanism and the emission of greenhouse gases with consequent global warming. Measurements of gases vaulted in

Formattato: Italiano (Italia)

Formattato: Italiano (Italia)

Formattato: Italiano (Italia)

Formattato: Italiano (Italia)

calcite of end Permian brachiopods and whole rock document significant differences in normal atmospheric equilibrium concentration in gases between modern and end Permian seawaters. The gas composition of the end Permian brachiopod-inclusions reflects dramatically higher seawater carbon dioxide and methane contents leading up to the biotic event. Initial global warming of 8 to 11°C sourced by isotopically light carbon dioxide from volcanic emissions triggered the release of isotopically lighter methane from permafrost and shelf sediment methane hydrates. Consequently, the huge quantities of methane emitted into the atmosphere and the oceans accelerated global warming and marked the negative $\delta^{13}C$ spike observed in marine carbonates, documenting the onset of the mass extinction period. The rapidity of the methane hydrate emission lasting from several years to thousands of years was tempered by the equally rapid oxidation of the atmospheric and oceanic methane that gradually reduced its warming potential but not before global warming had reached levels lethal to most life on land and in the oceans. Based on measurements of gases trapped in biogenic and abiogenic calcite, the release of methane (of ~ 3-14% of total C stored) from permafrost and shelf sediment methane hydrate is deemed the ultimate source and cause for the dramatic life-changing global warming (GMAT > 34°C) and oceanic negative-carbon isotope excursion observed at the end Permian. Global warming triggered by the massive release of carbon dioxide may be catastrophic, but the release of methane from hydrate may be apocalyptic. The end Permian holds an important lesson for humanity regarding the issue it faces today with greenhouse gas emissions, global warming, and climate change.

1. Introduction

The end Permian was the greatest natural catastrophe experienced by life on Earth with its impact recorded in terrestrial and marine rock archives. About 90% of marine species, 70% of terrestrial vertebrate species, 30% of insect orders and an indeterminate percentage of terrestrial and marine plants succumbed during this catastrophe (e.g., Erwin, 1994; Brand et al., 2012). This devastating mass extinction on Earth became the foundation for the rise of Mesozoic marine and terrestrial life. Important considerations of the end Permian mass extinction are documented by a dramatic and global negative carbon isotope excursion (Fig. 1) and, 1) the close connection in the demise of the marine

and terrestrial fauna and flora (e.g., Schneebeli-Hermann et al., 2013), 2) the rapidity of the onset of this catastrophe (e.g., Brand et al., 2012) and, 3) the tight age constraint for the end Permian extinction event (e.g., Burgess et al., 2014). Numerous causes have been proposed for the catastrophic end Permian mass extinction, which may have acted alone or in concert, but with many researchers favoring a tangled web of interacting and related causes and effects such as global warming, anoxia and/or acidification (e.g., Wignall and Hallam, 1992; Cao et al., 2009; Clarkson et al., 2015). This global event is increasingly associated with the Siberian Trap volcanism and emission of the greenhouse gas CO_2 leading to global warming (e.g., Svensen et al., 2009; Schneebeli-Hermann et al., 2013). Some suggest that methane from a variety of sources may have played a supporting role (Berner, 2002; Retallack and Jahren, 2008; Brand et al., 2012), while oceanic anoxia was a minor and/or local player (e.g., Brand et al., 2012; Garbelli et al., 2015), and acidification only played a role during the Early Triassic (e.g., Clarkson et al., 2015).

Carbonates may contain gas trapped in minuscule inclusions that are readily released during crushing and subsequently may be analyzed by mass spectrometer for their gas make-up and compositions (e.g., Blamey, 2012). If the gases in these inclusions were trapped during formation/precipitation of the carbonate and remained sealed/vaulted in the inclusions, then they may represent seawater-dissolved gas, and with Henry's Law and mass balance calculations, we may establish a link between the hydrosphere and atmosphere (Brand et al., 2015b). Brachiopods are ideal archives because they precipitate low-Mg calcite shells that are resistant to post-depositional alteration (Brand and Veizer, 1980; Brand, 2004), and they incorporate carbon and oxygen isotopes into shell calcite in or near equilibrium with ambient seawater (cf. Lowenstam, 1961; Brand et al., 2013, 2015a). Furthermore, to reflect ambient environmental oceanographic conditions, biogenic carbonates including brachiopods must incorporate dissolved gases and water into shell calcite inclusions from seawater without modification of the normal atmospheric equilibrium parameters (NAEC; Fig. 2). Inclusions, microstructural defects manifested as pore, in modern brachiopods (Griesshaber et al., 2007, fig. 2; Goetz et al., 2009, fig. 2b) and in the end Permian brachiopod *Comelicania* sp. indet. (Fig. 3) may be quite small. Even smaller pores (nanostructural defects) are observed in some brachiopod shells (Fig. 4a) and probably quite applicable to the micron-sized micrite in whole rock,

are sufficiently ubiquitous (Fig. 4b) to satisfy the volume requirements demanded by the standard operating protocol of the analytical crush fast-scan mass spectrometry (CFS-MS) method for measuring trapped gases in inclusions. Gas and fluids with dissolved gas may be trapped during the depositional growth phase and/or the early diagenetic stage degradation of the organic tissue covering brachiopod fibers and micrite crystallites (Emig, 1990).

Our objectives are, 1) to characterize the gases in modern brachiopods and coral and use them as references and baselines for evaluating gases measured in the end Permian brachiopod shells and whole rock, 2) decipher the atmospheric and oceanographic conditions leading up to the end Permian event, and 3) identify the ultimate source/trigger for the catastrophic global warming and climate change event during the biggest mass extinction in Earth history.

2. Material and methodology

2.1. Sample material

Specimens of the modern brachiopod *Magellania venosa* were collected at the jetty in Huinay, Chile in Comau Fjord, and other modern shallow water brachiopods and corals were collected at Friday Harbor, Washington State and Signy Island, Antarctica (Brand et al., 2013) and from Indonesia (Azmy et al., 2010). The fossil shallow-water brachiopods and whole rock were collected from the uppermost Permian Bulla Member of the Bellerophon Formation and Tesero Member of the Werfen Formation, northern Italy (Brand et al., 2012).

2.2. Microstructural analysis

All material was cleaned of surface contaminants and the periostracum, while fossil brachiopods were extracted from the enclosing whole rock, and further cleaned by physical and chemical means (cf. Brand et al., 2012). Fossil brachiopods were cut longitudinally and thin sectioned for etching with 5% HCl for 20s and subsequent metallic coating. Microstructures were investigated with a Cambridge S-360 scanning electron microscope (SEM) at an accelerating voltage of 20 kV.

To visualize the presence of micro- (> 1 µm) and nanopores (< 1 µm) created by degradation of biopolymer membrane and fibrils in modern brachiopods, shell fragments were mounted on 3 mm thick cylindrical aluminium rods. The samples were then cut with a Leica Ultracut ultramicrotome with glass knifes to obtain a plane surface. Subsequently, surfaces were polished with a Diatome diamond knife by stepwise removal of layers with successively decreasing thicknesses (90 nm, 70 nm, 40 nm, 20 nm, 10 nm and 5 nm; each step was repeated 15 times). The highly even surface was etched between 90 and 120 seconds with a 0.1M HEPES solution adjusted to a pH of 6.5. Etching of the carbonate mineral was accompanied by fixation of organic components with a solution of 2.5% glutaraldehyde. Etching and fixation was completed by dehydration of samples in 100% isopropanol alcohol; 3 times for 10 seconds each. Subsequently shells were critically point dried in a BAL-TEC CPD 030 (Liechtenstein), then rotary coated with 3 nm of platinum and imaged at 4kV using a Hitachi S5200 field-emission scanning electron microscope (FE-SEM).

Biopolymer decomposition was carried out with laboratory-based hydrothermal alteration. Shell pieces were placed in a Teflon liner together with 25 mL of meteoric solution. Subsequently, the liner sealed with a Teflon lid was introduced into a stainless steel autoclave, sealed again, and placed in an oven at 175ºC for 14 days. This laboratory procedure quickly destroys the organic tissue covering the fibers and the organic fibrils within them, and gaps and voids between and within the fibers become readily visible (cf. natural decomposition, Emig, 1990; Supplementary Figs. 1, 2).

Samples were also inspected by cathodoluminescence (CL) using a Nuclide ELM2 cathode luminoscope operating at 10 kV and 5-7 mA. Trace chemistry and stable isotope analyses and results are well described in Brand et al. (2012).

2.3. Analytical gas method

Modern and fossil brachiopods and whole rock were measured for inclusion gas in their calcite fibers (secondary layer) and columns (tertiary layer) by mass spectrometry. Extraction and analysis of volatiles was performed by the crush-fast scan (CFS) method (Norman and Blamey, 2001; Blamey, 2012), and at room temperature it offers low

detection limits (1.2e-15 mol, 2σ) with negligible blank readings (< 4.14e-14 mols CH_4 to > 1.0e-16 mols Ar).

Prior to analysis, the crushing area and bellows of the crusher were cleaned with potassium hydroxide. Any potassium hydroxide residue was removed by swabbing with deionized water, followed by an isopropanol wash and air-drying. Subsequently, the crushing chamber was baked at 150°C for 72 hours prior to loading the first sample. Furthermore, the mass spectrometer's (MS) chamber was baked-out at 150-200°C overnight followed by cooling to room temperature prior to analysis of samples. The MS chamber is isolated from the crushing area that holds the sample material, which affords the ability to bake out the former every evening. This procedure prevents heating of samples in the crushing chamber while allowing the removal of gas adhering to or trapped interstitially in the sample material by vacuum pumping.

Samples the size of a match head (e.g., ~100 mg) were cleaned with KOH then air-dried at room temperature. Samples were then loaded into the crushing chamber and held under vacuum (~10^{-8} Torr) for 18 hours. During the analysis phase, samples were crushed in swift increments, with each crush producing a burst of mixed volatile gas that is individually analyzed. A typical sample size of about 100 mg (one or two 3-mm grains) releases four to ten bursts of volatile gas (up to ~2×10^{-11} mol) into the MS vacuum chamber, where it remains for 8–10 analyzer scans (~2 seconds) before removal by turbo pump. This method does not require a carrier gas and volatiles are not separated from each other but released simultaneously into the chamber.

The MS was calibrated using Scotty Mini-mix commercial standard gas mixture, synthetic inclusions filled with gas mixtures, and three in-house fluid/gas inclusion gas standards as described by Norman and Blamey (2001). The Mini-mix gas mixture has a 2% error in the value of the secondary gas mixed with nitrogen.

Detection limits are described, in detail, for the analytical process by Blamey et al. (2012). The analytical error (one sigma) is determined from multiple analyses of the NB-84 internal standard for carbon dioxide (Appendix). Errors for other gases are determined by multiplying the CO_2 error by the ratio of the CO_2 sensitivity factor (see Blamey et al., 2012) and by the sensitivity factors for the other gases. Error relative to the reported value

for CO_2 of 13.0%, Ar is 11.4%, O_2 is 15.8%, N_2 is 7.1%, CH_4 is 8.2%, He is 11.6%, and H_2 is 3.0%.

Conversion of mass spectrometer current readings (amps) to gas concentration (moles) was achieved by analyzing the major gas contents of 1 µL capillary tubes containing atmosphere at lab temperature and pressure (Norman and Sawkins, 1987; Appendix). The tube was crushed in the crusher chamber in the same manner as the samples. The number of moles of nitrogen (obtained using PV = nRT) was equated to the measured current. The equivalence determined at the time of measurement of meteorites was 1680 amps per mole (Blamey et al., 2015). The uncertainty in measurement was less than 1.8%. Blank current was about double that of background current. The standard deviation of the mass spectrometer's signal to noise ratio at mass 15 background was 1.196e-13. Overall, analytical gas signals have precision of better than 0.5% (1σ), and gas content of internal standard NB-84 is within 1% of reported contents (Blamey et al., 2015).

Each sample gas burst was analyzed for H_2, He, CH_4, N_2, O_2, Ar, and CO_2, using two Pfeiffer Prisma "residual-gas" quadrupole mass spectrometers operating in fast-scan, peak-hopping mode at room temperature. A total of 37 gas measurements were made on seven modern biogenic samples, and a total of 44 gas measurements were obtained on six end Permian brachiopod and whole rock samples. A total of 81 normalized gas measurements (weighted by gas burst size) reported in mol % are listed in the Appendix.

3. Diagenetic screening

The physical evidence supports the presence of suitable pores (Figs. 3, 4) but that is only the first step in the evaluation process. Furthermore, we must establish that the gas contents of brachiopod and other marine archives reflect NAEC of gases in seawater and consequently of the atmosphere. A plot of gas contents of several modern brachiopods and one coral shows that they indeed reflect equilibrium seawater and atmospheric compositions, which confirms their potential as archives of trapping environmental gases for paleo-atmospheric gas reconstructions (Fig. 2).

Preservation of fossil biogenic and abiogenic material must be established to document their reliability as carriers of NAEC gases. Petrographic (including CL),

microstructural, trace chemistry and stable isotope evaluations are conducted to assess the preservation state of carbonates (cf. Brand and Veizer, 1980). Microstructural evaluations of the end Permian brachiopod *Comelicania* show the excellent preservation of fibers within their secondary layer as well as that of the growth-increment marked calcite columns of the tertiary layer (Fig. 3). This suggests that the shells of the brachiopods are preserved in their original low-Mg calcite mineralogy (cf. Brand et al., 2012). In addition, the SEM micrographs show the presence of micropores (microstructural defects) in both types of calcite of the brachiopods; potential sites for trapped fluid and/or gas (Fig. 3). The supplementary figures allow for the precise positioning and context of the pores within brachiopods shells (Supplementary Figs. 1, 2).

Additional screening was carried out using trace element and stable isotope distributions. The Sr/Mn ratios suggest that all brachiopod samples are better preserved than their enclosing whole rock. In contrast, the carbon isotope composition with its higher resistance to alteration suggests that the selected brachiopods and whole rock are the most pristine (solid symbols, Fig. 5; Brand and Veizer, 1980). Furthermore, the similarity in the gas contents of the brachiopods and whole rock suggests that alteration (diagenetic, biochemical) was inconsequential for the six archives chosen from the end Permian of northern Italy (Fig. 6).

4. Gas classification

Further screening was conducted to test for the reliability in retaining NAEC of gases with the passage of time in the carbonates. Gas results of modern brachiopods plot in an area characterizing marine conditions in equilibrium with the atmosphere defined by CO_2/CH_4 ratios ranging from 10 to 1000, and by N_2/Ar ratios ranging from 35 to 130 (Table 1, Fig. 6), on the modified gas classification scheme originally proposed by Norman and Moore (1999) and Moore et al. (2001). Field boundaries have been constructed to accommodate ranges of gas measured in modern marine biogenic and abiogenic carbonates (1), for fresh-water carbonates (2), as well as carbonates that have experienced post-depositional (diagenetic) alteration (3), and gas concentration variations in marine carbonates with changes in atmospheric (seawater) chemistry and water salinity

and temperature (4), and changes in seawater chemistry influenced by bacterial carbonate reduction (Field 5, Fig. 6).

In contrast to the modern biogenic carbonates (Field 1), the end Permian brachiopods and whole rock from northern Italy plot into Field 4 designated modified Marine [change in chemistry] characterized by secular changes in seawater and atmospheric gas chemistry (Fig. 6). By virtue of their excellent preservation and constrained by their gas values within Field 4, the gas results from the end Permian samples should reflect ambient seawater/atmospheric conditions during time of formation.

5. Carbon Isotope Excursion (CIE)

The negative carbon isotope excursion (nCIE) in marine carbonates has been long recognized as an important marker of the end Permian (PT) event at Meishan, China and global localities, and it may vary by as much as 6.5‰ (Fig. 1; e.g., Jin et al., 2000; Retallack and Krull, 2006; Brand et al., 2012; Garbelli et al., 2015). However, its origin, source and duration remain problematic (Berner, 2002), and consequently, a definitive cause and mechanism for the nCIE and PT event still eludes us. A recent study by Burgess et al. (2014) provided more precise ages, and thus improved times for the onset, duration and offset of the mass extinction event that are essential in better understanding the reorganization of the carbon cycle and identifying a potential source for the trigger and kill mechanisms. Burgess et al. (2014) suggested, depending on sedimentation rate, the negative CIE shift and its rebound lasted between 2.1 to 18.8 thousand years, while slightly pre-dating the onset of the maximum extinction (cf. Brand et al., 2012).

5.1. Meishan – northern Italy nCIE Trend

In conjunction with results from Meishan, precisely placed and well-preserved samples from the end Permian succession in northern Italy provide the requisite high-resolution database (Brand et al., 2012) to shed more light on the cause of the greatest mass extinction. Gas ratios of the end Permian samples fall into Field 4 (marine carbonates with changing chemistry, Fig. 6), and with methane dominating the greenhouse gas content relative to that of modern counterparts (Tables 1, 2). A closer examination of the time interval preceding the mass extinction clearly shows a negative

CIE of about 3.5‰ leading up to the major event at Meishan, and in part, in northern Italy (Fig. 7A), while a smaller but distinct negative $\delta^{13}C$ excursion in the lower half of bed 24e at Meishan is also recognized in the results from Italy (Fig. 7B; cf. Brand et al., 2012). These two negative carbon isotope excursions are designated 'Pulse 1' and 'Pulse 2', which also correspond to negative excursions of the brachiopod $\delta^{18}O$ values from Italy (Fig. 7C, expressed in T°C). Based on the $\delta^{18}O$ values of conodonts, water temperatures at Meishan remained around 25°C and reached higher ones only during deposition of Bed 26 and subsequent beds (Joachimski et al., 2012), whereas those from northern Italy based on shallow water brachiopod *Comelicania* ranged from 30°C up to 35°C just before the extinction (Fig. 7C; Brand et al., 2012). The water temperatures associated with Pulse 2 are sufficiently high (GMAT, Table 3) to cause stress for many tropical and polar organisms because of their poor acclimation capacity (e.g., Stillman, 2003; Peck et al., 2010), leading to widespread lethal environmental conditions and possibly mass die-off.

The measured CO_2/CH_4 ratios of the end Permian samples are relatively low (Table 2) and essentially invariant but marked by two distinct pulses corresponding to the negative carbon and oxygen isotope excursions and warming trend pulses noted at Meishan and northern Italy (Fig. 7D). The first gas pulse corresponds to the small but significant nCIE noted in the lower half of Bed 24e at Meishan and to corresponding levels in northern Italy (Fig. 7A, B). The subsequent rise in the gas ratio may be related to the rapid oxidation of some of the released methane to carbon dioxide (Berner, 2002). The second pulse and more pronounced fall in the CO_2/CH_4 ratio document a significant upswing in methane emission just before the onset of the end Permian biotic crisis, which corresponds well with the world-wide observed nCIE and water temperature changes observed in northern Italy and Tibet (cf. Brand et al., 2012; Garbelli et al., 2015).

6. End Permian atmospheric conditions

Generally, uncertainties of timing and duration of events limit the interpretations of many important biologic/geologic events, including the end Permian mass extinction (e.g., Rampino et al., 2000; Posenato, 2009; Shen et al., 2010). But this critical issue of time has been resolved with results from recent publications that allow for the improved geochemical characterization of the source(s) for this most dramatic event (Brand et al.,

2012; Joachimski et al., 2012; Burgess et al., 2014). The issue of ambient gas content and concentration is resolved by the crush fast-scan method that measures gas trapped in tiny pores of select modern and fossil materials reflecting marine and atmospheric systems (Tables 1, 2; cf. Brand et al., 2015a). Consequently, only the best material with preserved NAEC of gases in seawater will be used in characterizing the end Permian atmosphere (Field 4, Fig. 6).

The greenhouse gas build-up prior to the PT event was driven by carbon dioxide emitted by Siberian Trap volcanic deposits (e.g., Svensen et al., 2009), and methane emission from hydrates/clathrates is a leading contender for 'pushing' the global warming process over the sustainable limit (e.g., Retallack and Jahren, 2008). Armed with pre-industrial atmospheric conditions, we note a gradual but rising shift in both CO_2 and CH_4 by the 1980's (Table 3). This time interval clearly defines the relationship between atmospheric and marine hydrospheric conditions and those of the ambient biogenic and abiogenic marine carbonates.

6.1. Model and measured parameters

A number of researchers modeled gas ratios for the end Permian (e.g., Berner, 2002; Kiehl and Shields, 2005; Retallack and Jahren, 2008; Brand et al., 2012) with contents ranging from 1700 ppm to 3550 ppmv for CO_2, and 'constant' 0.7 ppmv for CH_4 (during the end Perm (a), end Perm (d1), Table 3). A supplemental parameter of fixed CO_2 and variable CH_4 is added to the discussion and this segment (end Perm (c), Table 3). There are potentially a number of concerns with these modeled atmospheric parameters, such as, 1) the mean global atmospheric temperatures derived from these parameters may not be high enough to bring about a biotic crisis, and 2) there was insufficient negative carbon to produce the world-wide observed nCIE at the end Permian (e.g., Berner, 2002).

Two modeled parameters, 1 (end Perm (a), Table 3) and 2 (end Perm (b), Table 3), assume no change or contribution by methane to the global climate change scenario, and with $Brach_{ratios}$ (780 and 476) well above those measured in modern and end Permian counterparts. Clearly, the two-modeled parameters are outside the realm of possibility of the gas ratios measured in the end Permian brachiopods (Table 2). It is apparent that the inconsistency does not rest with the postulated CO_2 contents but with the methane

component, and consequently, alternatives to the constant and static CH_4 composition must be contemplated.

The third model parameters suggest conditions (end Perm (c), Table 3) equally unsatisfactory with proposed modern carbon dioxide levels but an increased methane component since the postulated global GMAT (20.3°C) is quite insufficient to trigger a biotic crisis. Furthermore, pH level with this atmospheric parameter (8.28) was unlikely to cause great concerns with oceanic acidification, unlike the ones calculated for the first two model conditions (7.64, 7.78, Table 3).

It has been proposed that CO_2 may have varied for the end Permian between 1700 and 3500 ppm (Table 3). With an atmospheric ratio of 27.8 based on the average brachiopod ratio of 4.3 determined for the end Permian, we are able to determine the methane concentration during the end Permian. In this instance, CH_4 may have varied between a low of about 61 (pre-Pulse) and a high of about 245 ppmv (Pulse 2) with corresponding amounts of carbon dioxide (Table 3). Global temperature and seawater pH levels are sufficiently high and low, respectively, and with these postulated gas parameters environmental conditions might be a challenge for terrestrial and marine life.

6.2. End Permian atmosphere

A detailed evaluation of the gas components and their trends suggests that during pre-Pulse time the brachiopod CO_2/CH_4 ratio was about 4.3, but during Pulse 1 it dropped to 3.3, and then to 2.2 during Pulse 2 with recoveries in between (Fig. 7D, Table 3). Maintaining the appropriate ratios and modeled atmospheric concentrations of carbon dioxide, the methane content of the atmosphere may have varied from a low of 61 ppmv during pre-Pulse time to 121 ppmv during Pulse 1 and increased to possibly 245 ppmv at the onset of the biotic crisis (Fig. 7D, Table 4). Considering the global warming potential of both CO_2 and CH_4, the Global Mean Air Temperature (GMAT) may have varied from 29 to 34°C, which correspond well to within several degrees to water temperatures recorded by tropical end Permian shallow-water brachiopods from northern Italy (Brand et al., 2012) and Tibet (Garbelli et al., 2015). The slight SST offset may be related to differences in currents, habitat morphology and depths of these shallow water brachiopods. Overall the temperature impact by methane would be significant but of short

duration because of its fast oxidation to carbon dioxide (Berner, 2002) as evidenced by the reversal in CO_2/CH_4 ratio just before Pulse 2 (Fig. 7D). In addition, the determined pH values of 7.85 to 7.69 are sufficiently low to suggest some acidification of seawater during this critical time period (Table 3).

7. Methane source

The question arises: is the emission of gas from Siberian Trap volcanism sufficient to cause both the exacerbated warming and negative carbon isotope shift experienced during the end Permian (Fig. 8a)? The answer on both accounts is in the negative (e.g., Berner, 2002; Retallack and Jahren, 2008; Brand et al., 2012), and thus a new question must be posed whether there is sufficient methane stored in permafrost and marine sediment, upon release, to cause a major perturbation of the global carbon cycle with subsequent warming and its accompanying nCIE (Fig. 8b). If the amount of methane in the atmosphere varied from 61 to about 245 ppmv based on gas measured in end Permian marine carbonates (Table 4), we should be able to determine the amount of stored isotopically light methane that would need to be released from these two reservoirs. With about 2800 Gt of C stored in the two major sinks of marine sediments and permafrost today (Kvenvolden, 1998; Boswell and Collett, 2011), and under present climatic conditions there has been a miniscule release of 0.1% methane hydrates over the last 100 years from marine sediments amounting to an atmospheric contribution of 1125 ppbv CH_4 (Table 4; Ruppel, 2011). We performed simple mass balance calculations of methane release for a period of 100 years and distributed these evenly among the permafrost and marine sediment reservoirs of methane hydrate. During the pre-Pulse stage atmospheric methane attained a level of about 61 200 ppbv (Table 4) and when combined with the emission rate of 1125 ppbv/100 years equal to 0.1% from methane hydrate gives a contribution of about 2.7% and 4.9% from the marine sediment and permafrost reservoirs, respectively, for a total mass of about 98 Gt C/100 years (Table 4). For Pulse 1, the amount of methane released would have been equivalent to about 5.4 and 9.7%, respectively, for a total contribution of 193 Gt C/100 years (Table 4). For Pulse 2, the amount of methane released would have been equivalent to about 10.9 and 19.6%, respectively, for a total contribution of about 392 Gt C/100 years (Table 4). These

contributions equate to yearly rates ranging from 1.0 to 3.9 Gt C (CH_4), which are similar to emission rates of 0.8 to 2.1 Gt C/y calculated for C-isotope depleted carbon dioxide derived from the experimental metamorphism of carbon rich sediments (Svensen et al., 2009). This process would be coeval to the release of gas by the Siberian Traps and not limited to just the 'end' of the Permian just slightly preceding the biotic event, and furthermore, it is not supported by the rapid onset of the well-documented nCIE (Figs. 1, 7).

It is clear from our discussion and the extensive literature that warming of the Earth was caused by carbon dioxide emission during Siberian Trap volcanism (Fig. 8). Eventually with major and sudden release of methane from hydrate during the end Permian, global temperatures reached levels detrimental to marine and terrestrial life, and its oxidized product (highly negative carbon dioxide) caused the prominent negative carbon isotope excursion documented in many global marine and terrestrial sequences (cf. Berner, 2002; Schneebeli-Hermann et al., 2013). Thus, the gas contents of inclusions measured in marine carbonates from the end Permian support the concept that methane released from permafrost and marine sediments was the major cause for the greatest biotic crisis (Fig. 8).

8. Conclusions

Biogenic and abiogenic carbonates from the end Permian succession in northern Italy carry inclusion gases that formed in normal atmospheric equilibrium between the ambient seawater and atmosphere. Gas measured in inclusions suggests two pulses of methane emission before the end Permian mass extinction event.

Carbon dioxide derived from Siberian Trap volcanism with its $\delta^{13}C$ value of about -6‰ would bring about a warming of about 6°C and a shift in marine carbonate $\delta^{13}C$ values by about -2‰. The rapid addition of isotopically lighter methane (~ -60‰) to the global atmosphere and hydrosphere would bump up the average global temperature to well above 29°C, and after oxidation the $\delta^{13}C$ signature in marine carbonates would record carbon isotope compositions ranging from -2 to -7‰.

The emission of carbon dioxide from volcanic deposits may have started the world onto the road of mass extinction, but it was the release of methane from shelf sediments

and permafrost hydrates that was the ultimate cause for the catastrophic biotic event at the end Permian.

Our observations on the global warming process, such as the release of massive amounts of carbon dioxide and subsequently followed by methane from hydrates, and their impacts on life during the end Permian may have important lessons for humanity and the problems associated with climate change in the 21st century.

Acknowledgements

We thank Dr. Fan-Wei Meng and an anonymous reviewer for their helpful comments on the manuscript, and Mike Lozon (Brock University) for drafting and constructing the figures. We also thank NSERC (No. 7961-15), NSF, Brock, Munich, Memorial, New Hampshire, Ferrara, Milano and Bologna Universities for financial support.

References

Azmy, K., Edinger, E., Lundberg, J., Diegor, W., 2010. Sea level and paleotemperature records from mid-Holocene reef on the North coast of Java, Indonesia. International Journal of Earth Sciences 99, 231-244.

Berner, R.A., 2002. Examination of hypotheses for the Permo-Triassic boundary extinction by carbon cycle modeling. Proceedings of the National Academy of Sciences 99, 4172-4177.

Berner, R.A., 2006. Carbon, sulfur and O_2 across the Permian–Triassic boundary. Journal of Geochemical Exploration 88, 416-418.

Blamey, N.J.F., 2012. Composition and evolution of crustal, geothermal and hydrothermal fluids interpreted using quantitative fluid inclusion gas analysis. Journal of Geochemical Exploration 116-117, 17-27.

Blamey, N.J.F., Parnell, J., Longerich, H.P., 2012. Understanding detection limits in fluid inclusion analysis using an incremental crush fast scan method for Planetary Science. 43rd Lunar and Planetary Science Conference, Book of Abstracts, p. 1035.

Blamey, N.J.F., Parnell, J., McMahon, S.M., Mark, D., Tomkinson, T., Lee, M., Shivak, J., Izawa, M., Banerjee, N., Flemming, R., 2015. Evidence for methane in Martian meteorites. Nature Communications 6, 1-7.

Blamey, N.J.F., Brand, U., Parnell, J., Spear, N., Lécuyer, C., Benison, K., Meng, F., Ni, P., 2016. Paradigm shift in determining Neoproterozoic atmospheric oxygen. Geology (in press).

Boswell, R., Collett, T.S., 2011. Current perspectives on gas hydrate resources. Energy and Environmental Science 4, 1206-1211.

Brand, U., 2004. Carbon, oxygen and strontium isotopes in Paleozoic carbonate components: an evaluation of original seawater-chemistry proxies. Chemical Geology 204, 23-44.

Brand, U., Veizer, J., 1980. Chemical diagenesis of a multicomponent carbonate system: 1, Trace elements. Journal of Sedimentary Petrology 50, 1219-1236.

Brand, U., Logan, A., Hiller, N., Richardson, J., 2003. Geochemistry of modern brachiopods: applications and implications for oceanography and paleoceanography. Chemical Geology 198, 305-334.

Brand, U., Posenato, R., Came, R.E., Affek, H., Angiolini, L., Azmy, K., Farabegoli, E., 2012. The end-Permian mass extinction: a rapid volcanic CO_2 and CH_4-climatic catastrophe. Chemical Geology 322-323, 121-144.

Brand, U., Azmy, K., Bitner, M.A., Logan, A., Zuschin, M., Came, R.E., Ruggiero, E.T., 2013. Oxygen isotopes and $MgCO_3$ in brachiopod calcite and a new paleotemperature equation. Chemical Geology 359, 23-31.

Brand, U., Azmy, K., Griesshaber, E., Bitner, M.A., Logan, A., Zuschin, M., Ruggiero, E.T., Colin, P.L., 2015a. Carbon isotope composition in modern brachiopod calcite: a case of equilibrium with seawater? Chemical Geology 411, 81-96.

Brand, U., Blamey, N., Griesshaber, E., Posenato, R., Angiolini, L., Azmy, K., Farabegoli, E., Came, R., 2015b. Methane Clathrate: Killer cause of Earth's greatest mass extinction. Geological Society of America Annual Meeting, Baltimore, Maryland, GSA Abstracts, Session 68-5, p. 179.

Burgess, S.D., Bowring, S.A., Shen, S.Z., 2014. High-precision timeline for Earth's most severe extinction. Proceedings of the National Academy of Science 111, 3316-3321.

Cao, C.Q., Love, G.D., Hays, L.E., Wang, W., Shen, S.Z., Summons, R.E., 2009. Biogeochemical evidence for euxinic oceans and ecological disturbance presaging

the end-Permian mass extinction event. Earth and Planetary Science Letters 281, 188-201.

Clarkson, M.O., Kasemann, S.A., Wood, R.A., Lenton, T.M., Daines, S.J., Richoz, S., Ohnemueller, F., Meixner, A., Poulton, S.W., Tipper, E.T., 2015. Ocean acidification and the Permo-Triassic mass extinction. Science 348, 229-232.

Emig, C.C., 1990. Examples of post-mortality alteration in recent brachiopod shells and (paleo) ecological consequences. Marine Biology 104, 233-238.

Erwin, D.H., 1994. The Permo-Triassic extinction. Nature 367, 231-236.

Garbelli, C., Angiolini, L., Brand, U., Shen, S.Z., Jadoul, F., Posenato, R., Azmy, K., Cao, C.Q., 2015. Neotethys seawater chemistry and temperature at the dawn of the end Permian mass extinction. Gondwana Research 35, 272-285.

Goetz, A.J., Griesshaber, E., Neuser, R., Lüter, C., Hühner, M., Harper, E., Schmahl, W.W., 2009. Calcite morphology, texture and hardness in the distinct layers of rhynchonelliform brachiopod shells. European Journal of Mineralogy 21, 303-315.

Griesshaber, E., Schmahl, W.W., Neuser, R., Pettke, T., Blüm, M., Mutterlose, J., Brand, U., 2007. Cystallographic texture and microstructure of terebratulide brachiopod shell calcite: an optimized materials design with hierachial architecture. American Mineralogist 92, 722-734.

Jin, Y.G., Wang, Y., Wang, W., Shang, Q.H., Cao, C.Q., Erwin, D.H., 2000. Pattern of marine mass extinction near the Permian–Triassic boundary in South China. Science 289, 432-436.

Joachimski, M.M., Lai, X., Shen, S.Z., Jiang, H., Luo, G., Chen, B., Chen, J., Sun, Y., 2012. Climate warming in the latest Permian and the Permian–Triassic mass extinction. Geology 40, 195-198.

Kiehl, J.T., Shields, C.A., 2005. Climate simulation of the latest Permian: implications for mass extinction. Geology 33, 757-760.

Kvenvolden, K.A., 1988. Methane hydrate — a major reservoir of carbon in the shallow geosphere? Chemical Geology 71, 41-51.

Le Treut, H., Somerville, R., Cubasch, U., Ding, Y., Mauritzen, C., Mokssit, A., Peterson, T., Prather, M., 2007. Historical overview of climate change. In: Solomon, S., Qin, D., Manning, M., Chen, Z., Marquis, M., Averyt, K.B., Tignor, M., Miller, H.L. (Eds.),

Contribution of Working Group 1 to the Fourth Assessment Report of the Intergovernmental Panel on Climate Change. Cambridge University Press, Cambridge, United Kingdom and New York, pp. 94-127.

Lowenstam, H., 1961. Mineralogy, O^{18}/O^{16} ratios, and strontium and magnesium contents of recent and fossil brachiopods and their bearing on the history of the oceans. Journal of Geology 69, 241-260.

Moore, J.N., Norman, D.I., Kennedy, B.M., 2001. Fluid inclusion gas compositions from an active magmatic hydrothermal system: a case of The Geysers geothermal field, USA. Chemical Geology 173, 3-30.

Norman, D.I., Blamey, N.J.F., 2001. Quantitative analysis of fluid inclusion volatiles by a two quadrupole mass spectrometer system. Proceedings, European Current Research on Fluid Inclusions XVI, Porto, Portugal, Abstracts, pp. 341-344.

Norman, D.I., Moore, J.N., 1999. Methane and excess N_2 and Ar in geothermal fluid inclusions. Proceedings: Twenty-fourth Workshop of Geothermal Reservoir Engineering, Stanford University, Stanford, California, January 22-24, 1999, pp. 233-240.

Norman, D.I., Musgrave, J.A., 1994. N_2-Ar-He compositions in fluid inclusions: indicators of fluid source. Geochimica et Cosmochimica Acta 58, 1119-1131.

Norman, D.I., Sawkins, F.J., 1987. Analysis of volatiles in fluid inclusions by mass spectrometry. Chemical Geology 61, 1-10

Peck, L.S., Morley, S.A., Clark, M.S., 2010. Poor acclimation capacities in Antarctic marine ectotherms. Marine Biology 157, 2051-2059.

Posenato, R., 2009. Survival patterns of macrobenthic marine assemblages during the end-Permian mass extinction in the western Tethys (Dolomites, Italy). Palaeogeography, Palaeoclimatology, Palaeoecology 280, 150-167.

Rampino, M.R., Projoph, A., Adler, A., 2000. Tempo of the end-Permian event: high resolution cyclostratigraphy at the Permian–Triassic boundary. Geology 28, 643-646.

Retallack, G.J., Jahren, A.H., 2008. Methane release from igneous intrusions of coal during the Late Permian extinction events. Journal of Geology 116, 1-20.

Retallack, G.J., Krull, E.S., 2006. Carbon isotopic evidence for terminal-Permian

Formattato: Italiano (Italia)

Formattato: Italiano (Italia)

methane outbursts and their role in extinctions of animals, plants, coral reefs, and peat swamps. Geological Society of America, Special Paper 399, 249-268.

Ruppel, C.D., 2011. Methane hydrates and contemporary climate change. Nature Education Knowledge 3, 29-38.

Schneebeli-Hermann, E., Kürschner, W.M., Hochuli, P.A., Ware, D., Weissert, H., Bernasconi, S.M., Roohli, G., ur-Rehman, K., Goudemand, N., Bucher, H., 2013. Evidence for atmospheric carbon injection during the end-Permian extinction. Geology 41, 579-582.

Shen, S.Z., Cao, C.Q., Zhang, Y.C., Li, W.Z., Shi, G.R., Wang, Y., Wu, Y.S., Ueno, K., Henderson, C.M., Wang, X.D., Zhang, H., Wang, X.J., Chen, J., 2010. End-Permian mass extinction and paleoenvironmental changes in Neotethys: evidence from an oceanic carbonate section in southwestern Tibet. Global and Planetary Change 73, 3-14.

Stillman, J.H., 2003. Acclimation capacity underlies susceptibility to climate change. Science 301, 65.

Svensen, H., Planke, S., Polozov, A.G., Schmidbauer, N., Corfu, F., Podladchikov, Y.Y., Jamtveit, B., 2009. Siberian gas venting and the end-Permian environmental crisis. Earth and Planetary Science Letters 277, 490-500.

Weiss, R.F., 1974. Carbon dioxide in water and seawater: solubility of non-ideal gas. Marine Chemistry 2, 203-215.

Wignall, P.B., Hallam, A., 1992. Anoxia as a cause of the Permian/Triassic extinction: facies evidence from northern Italy and the western United States. Palaeogeography, Palaeoclimatology, Palaeoecology 93, 21-46.

Yin, H.F., Zhang, K.X., Tong, J.N., Yang, Z.Y., Wu, S.B., 2001. The global stratotype section and point (GSSP) of the Permian–Triassic boundary. Episodes 24, 102-114.

Fig. 1. $\delta^{13}C$ excursion, faunal disappearances and gas compositions about the end Permian (GSSP section at Meishan, China). Atmospheric greenhouse gas was dominated by CO_2 prior to the event with a sudden surge in CH_4 during the latest stage leading into the event.

Stratigraphy of Meishan section is from Yin et al. (2001), whereas faunal decline and carbon isotope trend are from Jin et al. (2000), and duration of the mass extinction period is from Burgess et al. (2014).

Fig. 2. Normal atmospheric equilibrium contents of gases in seawater and associated modern biogenic carbonates. The NAEC line represents equilibrium contents (dissolved) of carbon dioxide in modern seawater at temperatures ranging from 0 to 40°C (Weiss, 1974). The SI, FH and I (black diamonds) are CO_2 contents of modern biogenic carbonates (brachiopods and coral) from Signy Island, Friday Harbor and Indonesia of shallow water depth (< 100 m; Table 1).

Fig. 3. Scanning electron micrographs of secondary and tertiary layers in the end Permian brachiopod *Comelicania* sp. indet. from northern Italy. (A) Close-up of well-preserved secondary layer fibers showing the typical keel and saddle outlines and micro pores (structural defects) that may contain dissolved gases and seawater trapped during precipitation of the carbonate. (B) Close-up of well-preserved tertiary layer stacked columns with growth brands (cf. Goetz et al., 2009) and micro pores (structural defects) formed during the low-Mg calcite formation process.

Fig. 4. High-resolution field-emission scanning electron micrographs of micro-and nano-structures within components of layers of modern brachiopods. (A) Close-up of gaps between fibers of the secondary layer in *Notosaria nigricans* created after hydrothermal removal of organic tissue. (B) Close-up and distribution of nanopores (arrows point to some pores) created by the hydrothermal removal of organic tissue in secondary layer fibers of *Notosaria nigricans*. Supplementary Figs. 1, 2 provide locality context.

Fig. 5. Diagenetic screening of the brachiopod and whole rock material from the end Permian Bellerophon and Werfen Formations, northern Italy. Sr/Mn and $\delta^{13}C$ values are used to discriminate between altered and preserved carbonates (cf. Brand and Veizer, 1980). Samples in solid colors were chosen for gas analysis based on preservation status (geochemical and microstructural evidence).

Fig. 6. Gas ratios of CO_2, CH_4, N_2 and Ar captured in vaulted pores of modern (C – Huinay, Chile; FH – Friday Harbor, USA; SI – Signy Island, Antarctica) and end Permian brachiopods and limestone of northeastern Italy (Table 2). Classification consists of five fields: Field 1 – Marine Carbonates: carbonates in gas equilibrium with seawater and atmosphere; Field 2 – Meteoric Carbonate: carbonates in gas equilibrium with freshwater system; Field 3 – Diagenesis: diagenetically altered material; Field 4 – modified Marine Carbonates: carbonates with gas ratios shifted due to changes in seawater chemistry; and Field 5 – modified Marine Carbonates: carbonates with gas ratios shifted due the change in seawater chemistry and bacterial carbonate reduction. Atmospheric CO_2/CH_4 – N_2/Ar ratio included for reference; general gas classification scheme and magmatic field are modified after Norman and Musgrave (1994).

Fig. 7. Details of $\delta^{13}C$ values, seawater temperatures, and gas content excursions at Meishan, China and northeastern Italy. Shaded field represents mass extinction period during the end Permian. Information: stratigraphy (Yin et al., 2001); column A: carbon isotope trends (China – Jin et al., 2000); column B: carbon isotope trend (northern Italy – Brand et al., 2012); column C: seawater temperatures (China – Joachimski et al., 2012; northern Italy – Brand et al., 2012); column D: changing CO_2/CH_4 gas ratios of this study. Pulses 1 and 2 correlate with trend in $\delta^{13}C$ values from China and northern Italy, seawater temperatures and measured CO_2/CH_4 gas ratios. Gas symbols as in Fig. 6.

Fig. 8. Sequence of events before and during the end Permian mass extinction. Panel a) represents extensive Siberian Trap Flood volcanism and emission of the greenhouse gas CO_2 leading to climatic warming, and panel b) documents the subsequent release of massive amounts of methane (CH_4) hydrate from permafrost and marine shelf sediments and increased global warming (cf. Tables 3, 4). The contribution of methane from either permafrost and/or marine sediments is open for debate. Note: GMAT – Global Mean Annual Temperature; SL – sea level.

Supplementary Fig. 1. High-resolution field-emission scanning electron micrographs of secondary layer features (fibers and interfiber organic tissue; arrows point to examples) in *Magellania venosa* (Chile; S1-A). Once rapidly cleared of organic tissue (S1-B), the high connectivity of the interfiber space makes this space unsuitable as a site for hosting inclusion gas since it would be pumped away during the sample degassing stage (see gas analytical method's section).

Supplementary Fig. 2. High-resolution field-emission scanning electron micrographs of secondary layer features in *Notosaria nigricans*. Thermal degradation rapidly removes the inter-fiber and intra-fiber organic tissues (arrows point to examples; S2-A; cf. Emig, 1990). Fig. 4A (main text) is a close-up of the inter-fiber pore space left behind by the vacated organic tissue. S2-C and S2-D (Fig. 4B main text) are close-ups of nanopores noted in the fibers of *Notosaria nigricans* left behind by the removed biopolymer fibrils.

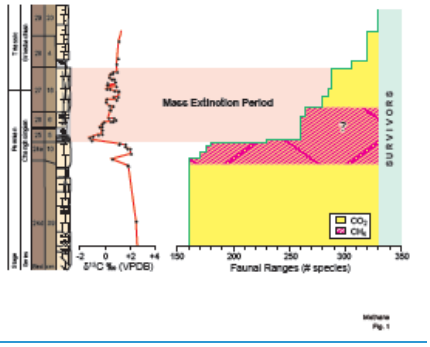

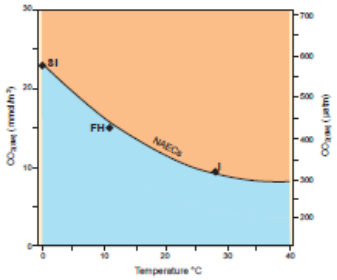

Methane
Fig. 3

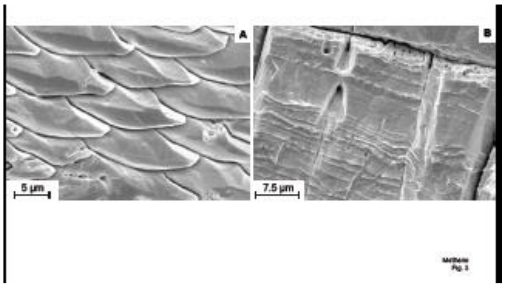

Methane
Fig. 1

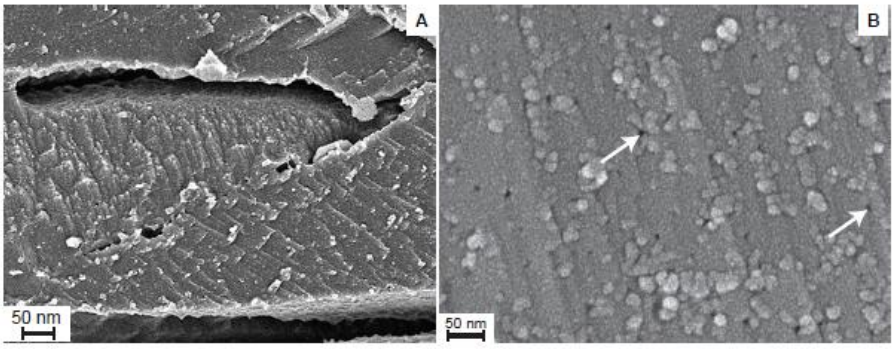

Methane
Fig. 4

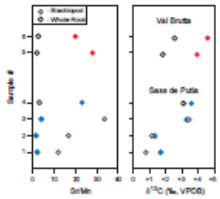

Methane
Fig. 5

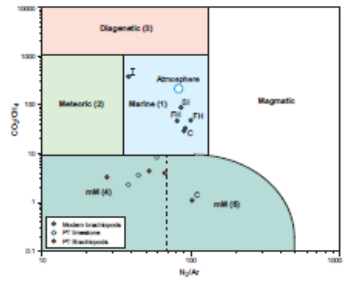

Methane
Fig. 6

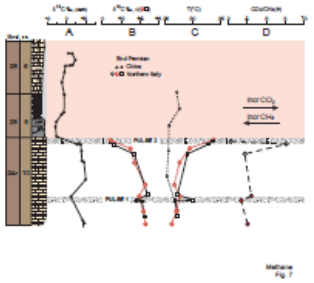

Methane
Fig. 7

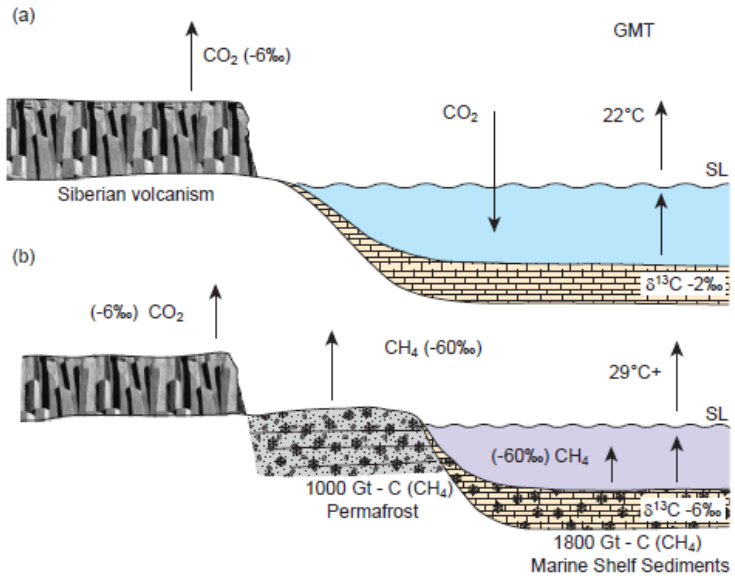

Table 1. Summary of weighted-mean gas concentrations (mol %) and ratios from gas inclusion measurements (Blamey, 2012; Blamey et al., 2015) of modern coral (I) and brachiopods (SI, FH1, FH2, C1, C2, C3; Brand et al., 2003; Appendix).

Sample	I	SI	FH1	FH2	C1	C2	C3	GMean
N	5	7	7	6	5	5	2	
T°C	28	0	10	10				
H_2	0.0	0.0614	0.0116	0.0603	0.2954	0.1195	2.2621	
He	0.00002	0.0001	0.0	0.0	0.0001	0.0	0.0004	
CH_4	0.00149	0.0222	0.0285	0.0302	0.1067	0.1420	2.0501	
H_2O	99.196	97.1760	97.2698	98.7821	92.2203	93.2831	90.1030	
N_2	0.1743	0.7495	1.2063	0.1212	3.6510	3.3627	3.2046	
O_2	0.0378	0.0334	0.0990	0.0064	0.0583	0.0500	0.0149	
Ar	0.0046	0.0087	0.0120	0.0013	0.0404	0.0415	0.0315	
CO_2	0.5811	1.9487	1.3727	0.9984	3.6278	3.0012	2.3333	

CO_2/CH_4	390	87.8	48.2	33.1	34.0	21.1	1.1	33.1
N_2/Ar	37.9	86.1	100.5	93.2	90.4	81.0	101.7	80.9

Note: I – Indonesia; SI – Signy Island; FH1, FH2 – Friday Harbor; C1 to C3 – Huinay, Chile; N – number of gas measurements; T°C – ambient water temperature (Brand et al., 2013).

Table 2. Summary weighted-mean gas concentrations (mol %) and ratios from inclusion gas measurements (Blamey, 2012; Blamey et al., 2015) of end Permian (PT1, PT2, PT3) brachiopods and whole rock (PT wr-1 to wr-3; Brand et al., 2012, 2013; Appendix).

Sample	PT1 wpk-6	PT2 VB-8A	PT3 VB-9A1	PT wr-1 wpk-10A	PT wr-2 wpk-10B	PT wr-3 wpk-11A
N	6	4	11	8	7	8
H_2	0.0694	0.0164	0.0187	0.0	0.0	0.0001
He	0.0001	0.0001	0.0001	0.0002	0.0001	0.0004
CH_4	0.2704	0.4846	0.6932	0.3064	1.0147	0.3911
H_2O	98.3538	92.9998	95.5411	97.5477	88.6251	97.3123
N_2	0.3887	3.8314	0.6795	0.5974	1.6672	0.5741
O_2	0.0123	0.6797	0.0327	0.0618	0.2707	0.0400
Ar	0.0142	0.0574	0.0129	0.0134	0.0283	0.0150
CO_2	0.8910	1.9307	3.0217	1.1240	8.2544	0.8669
CO_2/CH_4	3.3	4.0	4.4	3.7	8.1	2.2
N_2/Ar	27.4	66.7	52.7	44.5	58.9	38.4

Note: N – number of inclusion gas measurements.

Table 3. Green House Gas (GHG) compositions for pre-Industrial and modern time (Le Treut et al., 2007) and during the end Permian transition with equivalent atmospheric contents related to CO_2/CH_4 gas ratios (geometric mean) in brachiopod calcite archives (Tables 1, 2) and to concurrent global mean annual temperature (GMAT, °C), seawater pH, and brachiopod-based oxygen-isotope end Permian temperatures (BoT).

Age	$CO_2/CH_{4(atm)}$	$Air_{atm\ ratio}$	$Brach_{ratio}$	GMAT	pH	BoT
Pre-	290/0.7					

Industrial						
20th Century	380/1.77	214.7	**33.1**	16.9	8.28	
Model parameters						
end Perm (a)	3550/0.7	5071	***780****	25.7	7.64	
end Perm (b)	2166/*0.7**	3094	***476****	23.5	7.78	
end Perm (c)	380/**13.7**	27.8	**4.3**	20.3±1.1	8.28	
Measured parameters						
end Perm (d1)	1700/**61.2**	27.8	**4.3**	28.9±1.7	7.85	
end Perm (d2)	3500/**125.9**	27.8	**4.3**	33.1±2.0	7.65	
Segments (end Permian)						
Pre-Pulse	1700/**61.2**	27.8	**4.3**	28.9±1.7	7.85	26.1±0.7
Pulse 1	2600/**120.9**	21.5	**3.3**	31.8±1.9	7.73	30.0±0.9
Pulse 2	3500/**244.8**	14.3	**2.2**	34.1±1.7	7.69	33.5±1.1

Note: end Perm (a) – end Permian boundary conditions for CO_2 and CH_4 (ppmv; Kiehl and Shields, 2005, table 1), modeled ratio*; end Perm (b) crisis CO_2 conditions from stomatal indices (Retallack and Jahren, 2008), end Perm (c) – atmospheric CO_2 and CH_4 (ppmv) compositions based on end-Permian brachiopod CO_2/CH_4 gas ratio (Table 1, Appendix); end Perm (d1, d2) – atmospheric CO_2 based on various sources (e.g., Berner, 2002, 2006; Brand et al., 2012) and CH_4 (ppmv) composition adjusted to maintain the end-Permian material-based CO_2/CH_4 gas ratios; for pre-Pulse and Pulses 1 and 2 stratigraphic locations see Fig. 5; numbers in **RED** – calculated parameter, **Green** – Table 1, and **Blue** – Table 2.

Table 4. Permafrost and marine sediment hydrates and contributions of methane to the atmosphere. Estimate of methane gas contribution to end Permian atmosphere.

Present			
CH_4 (ppbv)	% CH_4-hydrates	Mass CH_4 (Gt C)	References
	100 (marine seds)	1800	Boswell and Collett, 2011
	100 (permafrost)	1000	Kvenvolden, 1988
1125/100 years	0.1	1.8	Ruppel, 2011
end Permian			
CH_4 (ppbv)	% CH_4-hydrates (marine sediments)	% CH_4-hydrates (permafrost)	Total Mass CH_4 (Gt C)/100 years
61 200 (pP)	2.72	4.896	97.92
120 900 (P1)	5.37	9.672	193.44
244 800 (P2)	10.88	19.584	391.68

Note: pP – pre- Pulse, P1 – Pulse 1, P2 – Pulse 2.

Appendix: Gas inclusion chemistry of New Mexico lab air, internal standard NB-84, a modern coral and brachiopods, and end
Weighted mean gas (molar %) is normalized for gas burst volume (cf. Blamey, 2012; Blamey et al., 2015).

Sample #	7-1 microlitre air capillary tubes (New Mexico lab air; Bl			
Crush	9396a	9396b	9396c	9404b
N2	78,81	77,24	78,70	77,64
O2	20,11	21,70	20,37	21,29
Ar	1,07	1,06	0,93	1,07
Burst	1,59E-09	1,58E-09	1,75E-09	2,06E-09

Sample #	Internal Standard NB-84			
Crush	8722r	8722s	8722t	8722u
H2	0	0	0	0
He	0,0002	0,0001	0,0001	0,0001
CH4	0,2053	0,1516	0,1724	0,1893
H2O	74,5592	74,1069	72,0670	74,0495
N2	0,1218	0,1780	0,1673	0,1723
O2	0,0029	0,0025	0,0051	0,0044
Ar	0,0005	0,0006	0,0004	0,0004
CO2	25,1102	25,5603	27,5878	25,5839
Burst size	2,20E-06	0,00000141	7,08E-07	0,00000137
CO2/CH4				
N2/Ar				

Sample #	*Porites lobata*, Holocene coral, Indonesia (Azmy et al., 2			
Crush	8240b	8240c	8240d	8240e
H2	0,0000	0,0000	0,0000	0,0000
He	0,0000	0,0000	0,0000	0,0000
CH4	0,0011	0,0013	0,0015	0,0017
H2O	99,2532	99,2769	99,2200	99,2612
N2	0,2682	0,1910	0,1700	0,1264
O2	0,0509	0,0411	0,0352	0,0269
Ar	0,0053	0,0051	0,0046	0,0034
CO2	0,4180	0,4806	0,5642	0,5757
Burst	4,44E-07	0,00000061	0,00000131	0,00000131
CO2/CH4				

N2/Ar

Sample #	*Liothyrella uva (*MB-SI*)*, Signy Island, Antarctica (Branc			
Crush #	9061b	9061c	9061d	9061e
H2	0,3361	0,0373	0,1166	0,0752
He	0,0000	0,0002	0,0003	0,0000
CH4	0,0469	0,0424	0,0244	0,0087
H2O	95,8700	97,7708	95,6418	95,6221
N2	0,2763	0,4791	1,5774	1,1731
O2	0,0092	0,0217	0,1276	0,0587
Ar	0,0051	0,0055	0,0187	0,0142
CO2	3,4566	1,6431	2,4932	3,0480
Burst	2,69E-08	5,28E-08	1,92E-08	2,83E-08

CO2/CH4

N2/Ar

Sample #	*Terebratalia transversa* (MB FH-1) - Friday Harbor, Was			
Crush #	9062b	9062c	9062d	9062e
H2	0,0088	0,0006	0,0000	0,0000
He	0,0001	0,0000	0,0001	0,0000
CH4	0,0131	0,0178	0,0093	0,0078
H2O	96,8617	96,2839	98,4626	98,1114
N2	1,3403	2,2785	0,7772	0,4400
O2	0,1522	0,1576	0,0363	0,0090
Ar	0,0139	0,0240	0,0075	0,0034
CO2	1,6100	1,2375	0,7071	1,4285
Burst	1,16E-07	6,91E-08	4,21E-08	1,52E-08

CO2/CH4

N2/Ar

Sample #	*Terebratalia transversa* (MB FH-2) - Friday Harbor, Was			
Crush #	9063a	9063b	9063c	9063d
H2	0,0497	0,2303	0,0673	0,0390
He	0,0000	0,0001	0,0001	0,0000
CH4	0,0222	0,1185	0,0336	0,0163
H2O	99,0719	98,3970	98,7733	98,5549
N2	0,1007	0,1593	0,1330	0,1007
O2	0,0069	0,0111	0,0059	0,0035
Ar	0,0011	0,0024	0,0013	0,0012
CO2	0,7475	1,0813	0,9856	1,2844

Burst	1,32E-07	3,97E-08	0,00000011	1,45E-07
CO2/CH4				
N2/Ar				

Sample #	*Magellania venosa* (MB C-1) - Huinay, Chile			
Crush #	9018a	9018b	9018c	9018d
H2	0,3615	0,2425	0,1389	0,1489
He	0,0001	0,0000	0,0005	0,0000
CH4	0,1277	0,0660	0,0163	0,0540
H2O	93,0389	91,5013	89,8679	93,3553
N2	4,0557	4,4419	4,8549	2,3657
O2	0,0178	0,1798	0,0352	0,0155
Ar	0,0412	0,0502	0,0514	0,0279
CO2	2,3571	3,5182	5,0349	4,0327
Burst	1,92E-08	1,86E-08	7,64E-09	1,66E-08
CO2/CH4				
N2/Ar				

Sample #	*Magellania venosa* (MB C-2) - Huinay, Chile			
Crush #	9019a	9019b	9019c	9019d
H2	0,0229	0,0336	0,1341	0,1893
He	0,0000	0,0001	0,0001	0,0000
CH4	0,0570	0,0464	0,2081	0,1612
H2O	94,8126	92,6676	93,3914	92,6633
N2	3,1246	3,1703	2,5008	3,8577
O2	0,0718	0,0339	0,0266	0,0395
Ar	0,0352	0,0440	0,0305	0,0519
CO2	1,8759	4,0042	3,7084	3,0373
Burst	4,65E-08	9,57E-09	2,81E-08	2,8E-08
CO2/CH4				
N2/Ar				

Sample #	*Magellania venosa* (MB C-3) - Huinay, Chile		
Crush #	9020a	9020b	Weighted Mean
H2	2,1899	2,3165	2,2621
He	0,0009	0,0000	0,0004
CH4	1,6826	2,3272	2,0501

H2O	90,5720	89,7494	90,1030
N2	3,2697	3,1556	3,2046
O2	0,0169	0,0134	0,0149
Ar	0,0313	0,0317	0,0315
CO2	2,2367	2,4062	2,3333
Burst	1,01E-08	1,34E-08	
CO2/CH4			1,1381
N2/Ar			101,5911

Sample #	*Comelicania* sp. ind. (wPk-6 base) - Italy, end Permian (			
Crush #	9022a	9022b	9022c	9022d
H2	0,0599	0,0654	0,0723	0,0705
He	0,0001	0,0001	0,0001	0,0001
CH4	0,2199	0,2248	0,2320	0,2818
H2O	98,4890	98,4783	98,3859	98,3230
N2	0,3928	0,3487	0,3814	0,3636
O2	0,0144	0,0128	0,0129	0,0104
Ar	0,0133	0,0124	0,0135	0,0141
CO2	0,8106	0,8576	0,9018	0,9366
Burst	0,00000159	6,13E-07	6,52E-07	9,59E-07
CO2/CH4				
N2/Ar				

Sample #	*Comelicania* sp. ind. (VB-8A) - Italy, end Permian (Bran			
Crush #	9021a	9021b	9021c	9021d
H2	0,0066	0,0103	0,0180	0,1482
He	0,0001	0,0001	0,0001	0,0002
CH4	0,3721	0,5100	0,5195	0,8563
H2O	91,3027	94,7731	93,6422	83,1829
N2	5,5641	2,1414	3,2938	11,2510
O2	1,0206	0,3717	0,5751	1,8780
Ar	0,0749	0,0385	0,0509	0,1629
CO2	1,6590	2,1549	1,9003	2,5206
Burst	1,32E-07	1,45E-07	1,67E-07	1,43E-08
CO2/CH4				
N2/Ar				

Sample #	*Comelicania* sp. ind. (VB9A-1) - Italy, end Permian (Bra

Crush #	9023a	9023b	9023c	9023d
H2	0,0000	0,0000	0,0189	0,0135
He	0,0000	0,0000	0,0001	0,0001
CH4	0,2986	0,4184	0,6623	0,8869
H2O	97,1005	97,1446	96,3176	94,6637
N2	0,4807	0,4892	0,5625	0,9056
O2	0,0477	0,0321	0,0179	0,0452
Ar	0,0082	0,0078	0,0102	0,0154
CO2	2,0642	1,9078	2,4105	3,4695
Burst	4,35E-07	4,24E-07	1,95E-07	1,42E-07
CO2/CH4				
N2/Ar				

Whole Rock Samples

Sample #	WPK 10A (Brand et al., 2012)			
Crush #	9073a	9073b	9073c	9073d
H2	0,0000	0,0000	0,0000	0,0000
He	0,0001	0,0002	0,0002	0,0002
CH4	0,2308	0,4127	0,3465	0,3321
H2O	98,2832	97,0717	97,4274	96,7818
N2	0,2504	0,6253	0,5577	1,0775
O2	0,0188	0,0474	0,0472	0,1129
Ar	0,0072	0,0160	0,0119	0,0227
CO2	0,9329	1,4085	1,3357	1,3102
Burst	3,34E-07	1,41E-07	1,68E-07	1,14E-07
CO2/CH4				
N2/Ar				

Sample #	WPK 10B (Brand et al., 2012)			
Crush #	9074a	9074b	9074c	9074d
H2	0,0000	0,0000	0,0000	0,0000
He	0,0001	0,0000	0,0001	0,0001
CH4	0,5833	0,8966	1,0061	1,0742
H2O	88,4635	87,5776	88,7424	89,9017
N2	2,1275	1,8225	2,3621	1,9861
O2	0,3510	0,3722	0,3824	0,3103
Ar	0,0320	0,0333	0,0372	0,0317
CO2	8,4241	9,2756	7,3488	6,4761
Burst	2,84E-07	2,71E-07	2,14E-07	2,81E-07

CO2/CH4

N2/Ar

Sample #	WPK 11A (Brand et al., 2012)			
Crush #	9075a	9075b	9075c	9075d
H2	0,0002	0,0007	0,0000	0,0000
He	0,0003	0,0004	0,0004	0,0004
CH4	0,3374	0,3013	0,2860	0,3561
H2O	97,3854	97,9586	98,0462	97,5094
N2	0,7439	0,5294	0,4486	0,5838
O2	0,0850	0,0426	0,0327	0,0461
Ar	0,0183	0,0133	0,0113	0,0146
CO2	1,0279	0,7596	0,7148	0,8672
Burst	1,98E-07	4,51E-07	0,00000069	0,00000077

CO2/CH4

N2/Ar

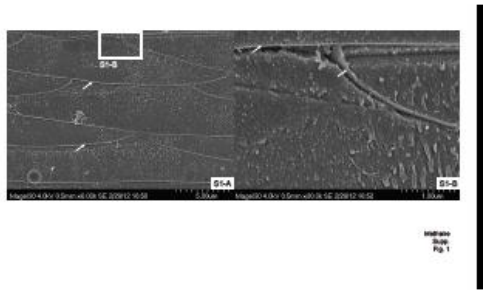

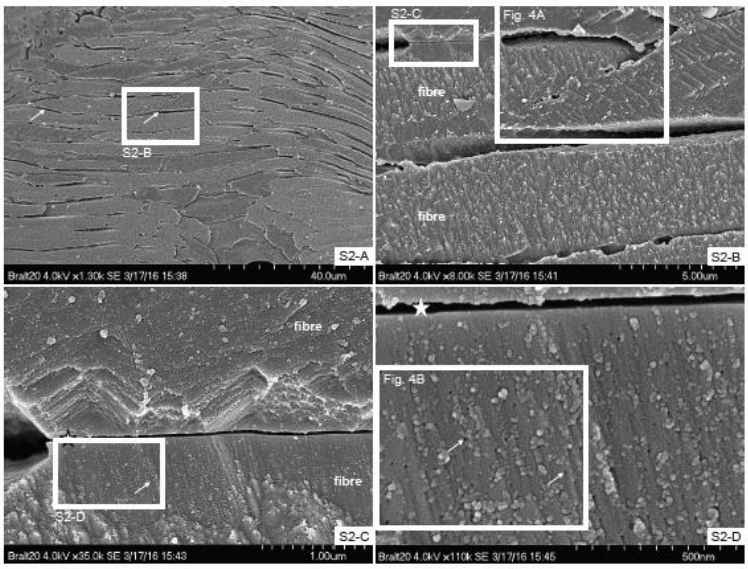

Methane
Supp.
Fig. 2